[6]Chorin, A. J., "Numerical Solution of the Navier-Stokes Equations," *Mathematics of Computation*, Vol. 22, No. 86, 1968, pp. 745-762.

[7]Chorin, A. J., "On the Convergence of Discrete Approximations to the Navier-Stokes Equations," *Mathematics of Computation*, Vol. 23, No. 90, 1969, pp. 341-353.

Expressions for k and ϵ Near Walls

Y.-H. Hwang* and T.-M. Liou†
National Tsing Hua University, Taiwan, Republic of China

Introduction

THE so-called wall functions have been widely used by the recent turbulence closure models in the prediction of wall-bounded shear flows. Certain distributions, e.g., the local heat transfer coefficient, are especially sensitive to the near-wall model. Consequently, a brief survey of previous formulas describing the near-wall distributions of the turbulence parameters would be worthwhile.

The logarithmic law for the mean-velocity distribution was derived by various researchers,[1,2] based on different hypotheses and highly supported by the experimental data.[3] Spalding[4] simplified the turbulent kinetic energy equation under three different cases, obtaining $k \sim y^{m_1}$ for the zero-shear layer, $k \sim$ constant for the constant-shear layer, and $k \sim y$ for the linear-shear layer. However, these solutions cannot be applied to the pipe axis or the edge of the boundary layer. In addition, Spalding did not provide solutions for ϵ, dissipation rate of the turbulent kinetic energy. Launder and Spalding[5] deduced $k = C_\mu^{-1/2}\tau_w/\rho$, $\epsilon \sim k^{3/2}/y$ and, consequently, the most widely used wall functions by an analysis of experimental data and by the rationale of the order of magnitude. The main assumption for the wall functions is the presence of an equilibrium layer where the generation and dissipation of k are in balance. No corresponding expressions relevant to the viscous sublayer and the outer layer were provided. El-Hawary and Nicoll[6] used empirical relations—$k = q(y^+/26)^{m_2}$ for $y^+ \le 26$, $k = q$ for $26 < y^+ < 70$, and $k = q(1 - y/\delta)$ for $y^+ > 70$—to represent the available experimental data in the entire boundary layer. Chieng and Launder[7] proposed a parabolic variation of k within the viscous sublayer, $k = k_v(y/y_v)^2$, based on a Taylor series expansion of the fluctuating velocity at the wall. The ϵ is not zero in the viscous sublayer, and has been shown by Pope and Whitelaw[8] to be constant equal to $2\nu_\ell(\partial k^{1/2}/y)^2$. By series expansion, Launder[9] and Patel et al.[10] also proposed $\epsilon = \epsilon_w + C_\epsilon y^2$ in the viscous sublayer, with ϵ_w and C_ϵ determined from experimental data. Recently, Wilcox[11] used the perturbation method to deduce $k \sim y^{3.23}$ and the specific dissipation rate $\omega = 6\nu_\ell/(\beta y^2)$ in the viscous sublayer.

The above literature survey reveals that most of the formulas for k and ϵ distributions close to the wall are either empirical or approximate, with the use of series expansion to represent the experimental data within a certain layer. There is lack of analytic expressions for both k and ϵ distributions in the near-wall region. The purpose of this paper is, therefore, to propose a set of algebraic relationships that attempt to model the near wall region of a turbulent boundary layer for the distributions of k and subsequent ϵ. The resulting expressions will be examined by the previous measurements and compared with previous derivations.

Received June 26, 1989; revision received March 3, 1990; accepted for publication April 16, 1990.

*Graduate Student, Power Mechanical Engineering Department.
†Professor, Power Mechanical Engineering Department.
Address correspondence to Prof. Tong-Miin Liou, Dept. of Power Mechanical Engineering, National Tsing Hua University, Hsin-Chu, Taiwan 30043, R.O.C.

Analysis

The governing equation of k for the boundary layer or the fully developed turbulent pipe flows can be simplified as follows:

$$\frac{d}{dy}\left[\left(\mu_\ell + \frac{\mu_t}{\sigma_k}\right)\frac{dk}{dy}\right] - \rho\overline{uv} - \rho\epsilon = 0 \tag{1}$$

In the following analysis, three turbulent models—$k-\epsilon$, $k-L$, and $k-\omega$—will be adopted to derive the distributions of k and ϵ in the near-wall region.

Analysis Based on the $k-\epsilon$ Model

In the fully turbulent region close to the wall, $\mu_\ell \ll \mu_t$, the Prandtl's mixing-length and the logarithmic mean-velocity profile give $\mu_t = \rho\kappa y U_\tau$. For $k-\epsilon$ model, one has $\epsilon = C_\mu \rho k^2/\mu_t$. If the Boussinesq's eddy viscosity concept is further adopted, Eq. (1) reduces to an autonomous equation

$$\frac{d}{dy^+}\left(y^+\frac{dk^*}{dy^+}\right) + \frac{\sigma_k C_\mu^{1/2}}{\kappa^2 y^+}(1 - k^{*2}) = 0 \tag{2}$$

with $k^* = C_\mu^{1/2}k/U_\tau^2$ and $y^+ = \rho U_\tau y/\mu_t$, and may be integrated to obtain

$$k^* = 3\left[\frac{(A_\pm y^+)^{\pm h^*} - 1}{(A_\pm y^+)^{\pm h^*} + 1}\right]^2 - 2 \tag{3}$$

for the inner branch (A_+; $+h^*$; $dk^*/dy^+ > 0$) and the outer branch (A_-; $-h^*$; $dk^*/dy^+ < 0$) of the equilibrium layer, respectively, where $h^* = (2\sigma_k)^{1/2}C_\mu^{1/4}/\kappa$. Note that the physical conditions, $k^* = 1$ and $dk^*/dy^+ = 0$, which result from assuming the presence of an equilibrium layer,[10] have been applied to determine the integration constants. The further constants A_+ and A_- can be determined by matching Eq. (3) with the solution for the viscous sublayer ($y_v^+ = 5.0$)

$$k^* = a_c C_\mu^{1/2} y^{+2} \tag{4}$$

and with $k^* = 0$[6] at the pipe axis or at the edge of the boundary layer, respectively. In deriving Eq. (4), the terms associated with μ_t and $-\rho\overline{uv}$ in Eq. (1) have been neglected and $\epsilon = 2\nu_\ell(dk^{1/2}/dy)^2$, proposed by Chieng and Launder,[9] has been adopted. The wall condition $k^* = 0$ has also been used. The constant a_c has a mean value of 0.045, recommended by Derksen and Azad.[12] It may be noted that the solution in Eq. (4) has the same form as that derived by Chieng and Launder[9] with the use of Taylor series expansion.

A combination of $\mu_t = \rho k y U_\tau$, $\epsilon = C_\mu \rho k^2/\mu_t$, and $\epsilon^+ = \mu_t \epsilon/(\rho U_\tau^4)$ leads to

$$\epsilon^+ = \frac{k^{*2}}{\kappa y^+} \tag{5}$$

for the near-wall region, where k^* is given by Eq. (3). Very near the wall, Patel et al.[10] proposed the empirical expression $\epsilon = \epsilon_w + C_\epsilon y^2$ for the viscous sublayer, which can be expressed as

$$\epsilon^+ = 2a_c + a_\epsilon y^{+2} \tag{6}$$

by the use of $\epsilon = 2\nu_\ell(dk^{1/2}/dy)^2$ and Eq. (4). The continuity of ϵ requires that Eq. (5) be equal to Eq. (6); thus, a_ϵ is determined.

Additionally, the dissipation term of the k equation in the $k-\epsilon$ model is usually computed by the following integration:

$$\overline{\epsilon^+} = \int_0^{y^+} \epsilon^+ dy^+ = \frac{1}{\kappa}\ell n(y^+/y_v^+) \pm (2/3)^{1/2}\frac{1}{\sigma_k^{1/2}C_\mu^{1/4}} \times [(k^{*3} - 3k^* + 2)^{1/2} - (k_v^{*3} - 3k_v^* + 2)^{1/2}] + 2a_c^2 y_v^+ + \frac{1}{3}a_\epsilon y_v^{+3} \tag{7}$$

Analysis Based on the $k-L$ Model

The eddy viscosity and ϵ can also be related to the length-scale L by the model,[13] $\mu_t = C_m \rho k^{1/2} L$ and $\epsilon = C_d k^{3/2}/L$. Equation (1) then becomes

$$\frac{d}{dy^+}\left(k^{*1/2}y^+ \frac{dk^*}{dy^+}\right) + \frac{\sigma_k C_\mu^{1/2}}{\kappa^2 y^+}(k^{*1/2} - k^{*3/2}) = 0 \tag{8}$$

Equation (8) is also an autonomous equation that can be easily integrated to obtain the solution of k^* for the inner branch (B_+; $+h^*$) and the outer branch (B_-; $-h^*$) of the equilibrium layer, respectively.

$$\frac{\{[6(k^*+1/2)]^{1/2} + 2k^{*1/2} + 1\}(1+k^*)}{\{[6(k^*+1/2)]^{1/2} - 2k^{*1/2} + 1\}(1-k^{*1/2})[(k^*+1/2)^{1/2} + k^*]\sqrt{6}} = (B_\pm y^+)^{\pm h^*/\sqrt{2}} \tag{9}$$

The matching conditions similar to those described previously further determined the values of B_+ and B_-. The distribution of ϵ can then be obtained from the above distribution of k by the use of $\epsilon^+ = k^{*3/2}/(\kappa y^+)$ and Eq. (6).

Analysis Based on the $k-\omega$ Model[11]

For an incompressible constant-pressure boundary layer, the k and ω equations of the $k-\omega$ model simplify to

$$\nu_t\left(\frac{dU}{dy}\right)^2 - \beta^*\omega k + \frac{d}{dy}\left[(\nu_t + \sigma^*\nu_t)\frac{dk}{dy}\right] = 0 \tag{10a}$$

$$\gamma\left(\frac{dU}{dy}\right)^2 - \beta\omega^2 + \frac{d}{dy}\left[(\nu_t + \sigma\nu_t)\frac{d\omega}{dy}\right] = 0 \tag{10b}$$

In the fully turbulent layer, the following relations can be resulted from comparing Eq. (10a) with Eq. (1) and comparing the definition $\nu_t = \gamma^* k/\omega$ in the $k-\omega$ model with $\epsilon = C_\mu \rho k^2/\mu_t$ in the $k-\epsilon$ model.

$$\omega = \epsilon/(\beta^* k), \qquad \sigma^* = 1/\sigma_k, \qquad \beta^*\gamma^* = C_\mu \tag{11}$$

From Eq. (11), and noting $\mu_t = \rho k y U_\tau$, Eq. (10a) is readily reduced to the autonomous Eq. (2). Consequently, both $k-\omega$ and $k-\epsilon$ model analyses lead to the same distributions of k and ϵ in the fully turbulent layer.

In the viscous sublayer, molecular diffusion and dissipation balance in Eq. (10) for perfectly smooth surfaces,[11] and this leads to

$$\omega = 6\nu_\ell/(\beta y^2), \qquad k = a y^{3.23}, \qquad \epsilon = 7.2\nu_\ell a y^{1.23} \tag{12}$$

where $k = ay^n$ has been postulated in this study, and the closure coefficients $\beta = 3/40$ and $\beta^* = 9/100$ are given by Wilcox.[11]

Results and Discussion

The derived distributions of k^* and ϵ^+ are plotted in Figs. 1 and 2, respectively, for both $k-\epsilon$ and $k-L$ models. In addition, comparisons are made with Laufer's data,[3] Spalding's theory,[4] and Wilcox's $k-\omega$ model.[11] Spalding's ϵ^+ curve in Fig. 2 is calculated by the authors from Spalding's k^* curve. It appears that the results predicted by the present expressions are generally in better agreement with Laufer's data than those predicted by Spalding's theory. Both $k-\epsilon$ and $k-L$ models provided similar results. The predictions of k^* and ϵ^+ are very accurate, except in the case of an overprediction of ϵ^+ in the viscous sublayer, where Wilcox's $k-\omega$ model shows much better agreement with Laufer's data without using wall functions or other approximations. Note that the $k-\omega$ model gives $\epsilon = 0$ at wall, a result different from $\epsilon_w \neq 0$ shown by other researchers, as addressed in the Introduction. The above overprediction in the viscous sublayer may be partly attributable to the incorrect ϵ measurements, as pointed out by Derksen and Azad;[12] but the recent paper by Mansour et al.[14] indicates the peak value of ϵ is less than Laufer's value. The smoothness of the curves and the good agreement between the curves and the experimental data, as shown in Figs. 1 and 2, also support the existence of an equilibrium layer in the near-wall region. Additionally, the matching conditions [$k^* = a_c C_\mu^{1/2} y^{+2}$, $y_\nu^+ = 5$) and ($k^* = 0$, $y = \delta$)] presented previously are independent of the Reynolds number. Hence, the curves shown in Figs. 1 and 2 have the feature of similarity. This observation is consistent with the well-known similarity of the mean velocity profile in the inner layer, overlap layer, and outer layer, respectively.

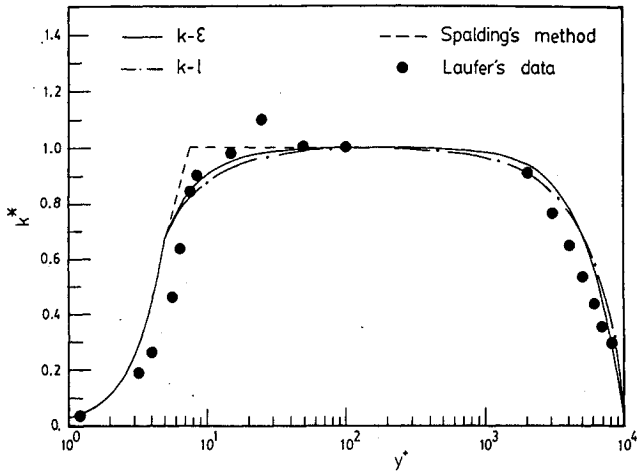

Fig. 1 Distribution of k^* near wall.

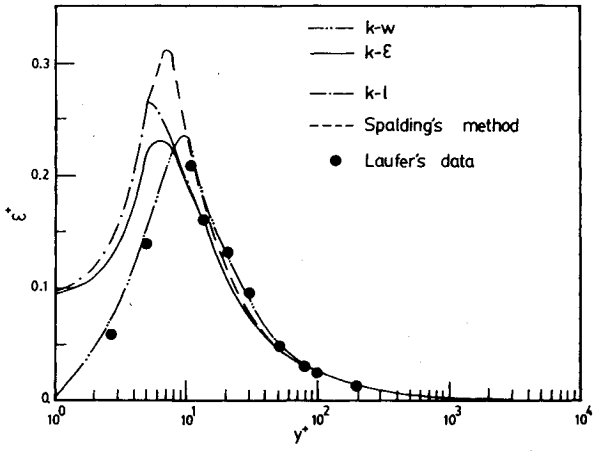

Fig. 2 Distribution of ϵ^+ near wall.

Conclusions

An analysis of the distributions of k and ϵ in the near-wall region that has been lacking in the past has been completed. The predictions with the current derived expressions are examined by comparing them with Spalding's derivation and with Laufer's data. The present expressions clearly show an improvement over Spalding's work in the predictions of the k and ϵ distributions from either the wall to the pipe axis or the edge of the boundary layer. The present expressions could be used in conjunction with two-equation turbulent models for numerical calculations. As for the viscous sublayer, it is found that Wilcox's $k-\omega$ model, without using wall functions, provides much better agreement with Laufer's data for ϵ. Furthermore, more accurate measurements of ϵ in the viscous sublayer are highly recommended for further work.

References

[1]Prandtl, L. "Uber die Ausgehildete Turbulenz," *ZAMM 5*, Birkhäuser Verlag, Basel, Switzerland, Sept. 1926, pp. 136-139.

[2]Van Driest, E. R., "On Turbulent Flow Near a Wall," *Journal of the Aeronautic Science,* Nov. 1956, pp. 1007–1011.

[3]Laufer, J., "The Structure of Turbulence in Fully Developed Pipe Flow," NACA TR-1174, Oct. 1954.

[4]Spalding, D. B., "Heat Transfer from Turbulent Separated Flows," *Journal of Fluid Mechanics,* Vol. 27, Jan. 1967, pp. 97–109.

[5]Launder, B. E., and Spalding, D. B., "The Numerical Computation of Turbulent Flows," *Computer Methods in Applied Mechanics and Engineering,* Vol. 3, March 1974, pp. 269–289.

[6]El-hawary, M. A., and Nicoll, W. B., "A Relation for the Length-Scale of Turbulent to Mean Flow Characteristics Close to the Wall," *Letters in Heat and Mass Transfer,* Pergamon, Vol. 7, Nov. 1980, pp. 401–411.

[7]Chieng, C. C., and Launder, D. B., "On the Calculation of Turbulent Heat Transport Downstream from an Abrupt Pipe Expansion," *Numerical Heat Transfer,* Vol. 3, April 1980, pp. 189–201.

[8]Pope, S. B., and Whitelaw, J. H., "The Calculation of Near-Wake Flows," *Journal of Fluid Mechanics,* Vol. 73, Jan. 1976, pp. 9–32.

[9]Launder, B. E., "Second Momentum Closure: Methodology and Practice," Proceedings of the Ecole d'Et'e d'Analyse Numerique-Modelisation Numerique de la Turbulence, France, 1982.

[10]Patel, V. C., Rodi, W., and Scheuerer, G., "Turbulence Models for Near-Wall and Low Reynolds Number Flows: A Review," *AIAA Journal,* Vol. 23, No. 9, 1985, pp. 1308–1319.

[11]Wilcox, D. C., "Reassessment of the Scale-Determining Equation for Advanced Turbulence Models," *AIAA Journal,* Vol. 26, No. 11, 1988, pp. 1299–1310.

[12]Derksen, R. W., and Azad, R. S., "Behavior of the Turbulent Energy Equation at a Fixed Boundary," *AIAA Journal,* Vol. 19, No. 1, 1981, pp. 238–239.

[13]Schlitchting, H., *Boundary Layer Theory,* McGraw-Hill, New York, 1979.

[14]Mansour, N. N., Kim, J., and Moin, P., *AIAA Journal,* Vol. 27, No. 8, 1989, pp. 1068–1073.

Three-Dimensional Visualization of Temporal Flow Sequences

I. van Cruyningen,* A. Lozano,* M. G. Mungal,† and R. K. Hanson‡
High Temperature Gasdynamics Laboratory
Stanford University, Stanford, California 94305

Introduction

FLOW visualization remains one of the most powerful methods of gaining insight into turbulent flow physics. Recently there have been several excellent reviews[1-3] that describe some of the latest developments in the field. It is also well known among the research community that movie or video sequences of flow visualization images, because of their dynamic nature, are frequently used to study flow development. Presentation of these data as a series of successive frame-by-frame images allows some correlation of temporal information, but is generally unsatisfactory as the human eye is much more adept at determining spatial correlations within a single image. This note describes the application of a method to generate single three-dimensional views that emphasize temporal correlations of time-evolving two-dimensional data sets (i.e. movies), thereby improve interpretation of such data.

Received Dec. 15, 1989; revision received Feb. 19, 1990; accepted for publication March 20, 1990.

*Research Assistant, Department of Mechanical Engineering.

†Assistant Professor, Department of Mechanical Engineering. Member AIAA.

‡Professor, Department of Mechanical Engineering. Member AIAA.

To generate the new views, the separate images are first stacked to form a data volume composed of the downstream spatial (x), cross-stream spatial (y), and time (t) dimensions. High-resolution volume rendering is used to extract constant property surfaces from this three-dimensional data volume. The resulting surfaces are shaded owing to a light source placed to the side of the viewing direction and projected onto the computer display. Temporal correlations, such as the movement of organized (coherent) structures, are then readily perceived. The method is illustrated with three specific examples of round jet flows: a forced low speed jet, a very high Reynolds number rocket motor exhaust jet, and a turbulent jet diffusion flame. It will be seen that, with volume rendering, interpretation of the flow physics is greatly improved, more so than was previously possible.

In related earlier work, Jimenez et al.[4] and Agui and Hesselink[5] stacked sequential cross-stream slices of a mixing layer and a low Reynolds number jet, respectively. Both of these data sets show y-z views of the flow at a fixed downstream station as a function of time t. Polygonal or cylindrical approximations to the surfaces were extracted from the y-z-t data volumes and were displayed with vector graphic techniques. The resulting images provided very useful information about the structures that are advected past the fixed downstream location. By contrast, in the present work, slices through the centerline of the flow are stacked to form x-y-t data volumes so that information for all downstream locations is available in one view. This perspective is found to be more amenable to studies of flow evolution.

Approach

In our work, an improved voxel-based (volume element) rendering algorithm[6] was used to reduce the data volumes on a PIXAR Image Computer with SUN 3/160C host. The algorithm operates on slices through the data volume with the light source direction and observation direction first selected. The slice orientation is then aligned with rays from the observation point to allow rapid final projection. Each slice and its two neighboring slices are mapped through a concentration threshold function, and the three-dimensional gradient of the mapped pixels is determined. The locations of the maximum magnitude of the gradient determine the rendered surface, whose normal is used to calculate the reflection of a collimated beam from the light source direction into the observation direction. Finally, the reflections from all surfaces in a given slice are summed towards the observation direction to produce one scan line for the display. Note that surfaces and normals are calculated at pixel resolutions so the rendered images retain the full resolution of the original data. No geometric approximations to the surface are made, which results in a faithful representation of the rendered surface.

To assist in understanding the fluid motion, depth cues due to shading are further enhanced by calculating numerous perspectives and allowing interactive rotation of the resulting views. The rotating volumes accentuate features observed in the static views presented here and are best observed directly on the computer screen or in video format.[7] Although, as discussed in Ref. 1, there is no effective way to archive video images in technical publications, volume renderings as used here may prove to be the next best substitute.

Results

Figure 1a illustrates a sequence of movie frames of a forced jet. These images were produced through a combination of planar laser-induced fluorescence and phosphorescence of a forced nitrogen jet flow[8] seeded with 5% mole fraction biacetyl (2-3 Butanedione). The jet issued at 85 cm/s (Re = 360) into a nitrogen coflow of 5.4 cm/s and was forced by a loudspeaker at 85 Hz (jet Strouhal number, St = 0.6) to produce the mushroom shaped vortical structures which convect downstream. Shown here are nine frames, each of 384 × 576 pixels, spanning one complete forcing cycle and seven down-